Fundamental Analysis of Vehicular Light Communications and the Mitigation of Sunlight Noise

Elizabeth Eso, *Member, IEEE*, Zabih Ghassemlooy, *Senior Member, IEEE*, Stanislav Zvanovec, *Senior Member, IEEE*, Juna Sathian, and Asghar Gholami

***Abstract*—Intelligent transport systems (ITS) rely upon the connectivity, cooperation and automation of vehicles aimed at the improvement of safety and efficiency of the transport system. Connectivity, which is a key component for the practical implementation of vehicular light communications (VeLC) systems in ITS, must be carefully studied prior to design and implementation. In this paper, we carry out a performance evaluation study on the use of different vehicle taillights (TLs) as the transmitters in a VeLC system. We show that, the transmission coverage field of view and the link span depend on TLs illumination patterns and the transmit power levels, respectively, which fail to meet the typical communication distances in vehicular environments. This paper proposes an infrared-based VeLC system to meet the transmission range in daytimes under Sunlight noise. We show that, at the forward error correction bit error rate limit of 3.8×10^{-3}, the communication distances of the proposed link are 63, 72, and > 89 m compared with 4.5, 5.4 and 6.3 m for BMW's vehicle TL at data rates of 10, 6, and 2 Mbps, respectively.**

***Index Terms*—Vehicular visible light communications, fundamental analysis, intelligent transport systems, infrared, sunlight noise.**

I. Introduction

THE WIRELESS exchange of traffic information between the vehicles and roadside infrastructure, which is part of the emerging intelligent transport systems (ITS), can significantly enhance the road safety and the efficiency of transportation networks [1]. ITS involves the provision of safe driving information, which include warning messages on the road terrains, pedestrian crossing the road, driving speed limits, etc. Presently, the radio frequency (RF) wireless communications technology is the established option in ITS, which is best known as the dedicated short-range communications (DSRC). DSRC supports several applications such as emergency braking warning and intersection collision warnings. However, some doubts still exist on the capability of DSRC in meeting the low latency and high reliability requirements in ITS considering both the network outages and security issues [2]. Consequently, considering the aforementioned issues, optical wireless communications (OWC) have emerged as an attractive and complementary technology in vehicular communications. It is interesting to note that, the OWC technology employing light emitting diodes (LEDs) gives rise to a smaller collision domain, which results in reduced packet losses due to interference, compared with the RF wireless systems [2]. Furthermore, the directionality of OWC increases the security of the communication networks, thus reducing the possibility of eavesdropping drastically.

The expanding multi-media-based services is the main driving force of the fifth generation (5G) and the emerging sixth generation (6G) and beyond wireless networks, which will be based on multiple technologies to ensure high quality of services [3]–[4]. OWC is envisaged to be part of 5G/6G and beyond wireless networks for use in application areas where RF-based technologies cannot be used due to insufficient bandwidth and other issues such as security, susceptibility to electromagnetic interference, etc. Several novel concepts on the use of OWC in 6G have been reported in [5], including (*i*) hybrid radio-optical wireless networks, where wireless nodes or devices are equipped with both RF and optical interfaces; and (*ii*) through-the-tissue optical communications, where very short ranges are considered to provide a highly secure link for intra-body and to/from body transmission. Note, the unique features of OWC that makes it an attractive technology for 5G/6G includes a large unlicensed spectrum, high security, high safety, lower power consumption, simplicity in implementation, low costs, and not susceptible to RF-induced interference. Consequently, the coexistence of the OWC and RF technologies can efficiently solve most of

Manuscript received July 23, 2020; revised November 12, 2020 and March 16, 2021; accepted April 25, 2021. Date of publication May 10, 2021; date of current version July 8, 2021. The work of Elizabeth Eso was supported by the European Union's Horizon 2020 Research and Innovation Programme under the Marie Sklodowska-Curie Grant 764461 (VISION). The work of Zabih Ghassemlooy was supported in part by the Engineering and Physical Sciences Research Council under Grant EP/P006280/1: MARVEL and in part by the EU COST Action Newfocus on optical wireless communications (CA19111). The work of Juna Sathian was supported in part by the Royal Society International Exchange Grant IES\R3\203061. The work of Stanislav Zvanovec was supported in part by the Czech Science Foundation Project GACR 17-17538S. The review of this article was coordinated by Prof. Yiqing Zhou. *(Corresponding author: Elizabeth Eso.)*

Elizabeth Eso, Zabih Ghassemlooy, and Juna Sathian are with the Optical Communication Research Group, Faculty of Engineering and Environment, Department of Mathematics, Physics and Electrical Engineering, Northumbria University NE1 8ST, U.K. (e-mail: elizabeth.eso@northumbria.ac.uk; z.ghassemlooy@northumbria.ac.uk; juna.sathian@northumbria.ac.uk).

Stanislav Zvanovec is with the Department of Electromagnetic Field, Faculty of Electrical Engineering, Czech Technical University, 166 36 Prague, Czech Republic, Czech Republic (e-mail: xzvanove@fel.cvut.cz).

Asghar Gholami is with the Department of Electrical and Computer Engineering, Isfahan University of Technology, Isfahan 84156-83111, Iran (e-mail: gholami@cc.iut.ac.ir).

Digital Object Identifier 10.1109/TVT.2021.3078576

the limitations of the individual RF and OWC links [6]. With the ever-increasing demand for internet of things, 5G is not guaranteed to meet up all the requirements of new services in the future [3], hence a hybrid/heterogenous system i.e., OWC with RF, enables 5G to be used in areas where RF cannot be utilised.

A growing number of research works on visible vehicular light communications (V-VeLC) have been reported in the literature. In [7], an analytical model for the bit error rate (BER) performance as a function of the communication distance for V-VeLC under different communication geometries and using a headlight (HL) beam pattern model was reported. It was shown that, (*i*) there were sharp degradations in the BER performance distribution to the left-hand side in the vertical plane, which is due to the asymmetric beam pattern of the low beam HL; and (*ii*) an increase in the achievable transmission link span provided the optical receiver's (Rx's) i.e., the photodiode (PD) and HLs heights were about 0-0.2 and 0.66 m, respectively. In [8], a comprehensive channel modelling to evaluate the performance of V-VeLC employing the high beam HL as the transmitter (Tx) under the weather conditions (rain and fog) was carried out. Using advanced ray tracing a path loss model in terms of transmission range was developed, showing the link span dropping from 72 to 26 m in the presence of heavy fog at a target BER of 10^{-6}. A 2×2 multiple-input multiple-output channel under Sunlight using a market-weighted HL pattern source as the Tx was studied in [9]. It was shown that, direct current biased optical orthogonal frequency division multiplexing (DCO-OFDM) offered higher data rates compared with the asymmetrically clipped optical OFDM (ACO-OFDM). with lower BER performance.

It is important to note that, most works reported on V-VeLC including the aforementioned references have considered high- or low-beam HLs, which are usually on during the night or under reduced visibility conditions (i.e., rain or fog). For the HLs, the transmit power P_T levels during daytime are relatively very low compared with the high- and low-beam lights used for road illumination. In [10], an extensive optical radiation pattern measurement of a single HL and TL was carried out. Several vehicle mobility traces with two-dimensional locations were also collected. Both data were combined to perform analytical study and to further obtain experimental distributions of the received power for HL- and TL-based Txs. Consequently, the issue of link asymmetry due to the significant differences in the radiation characteristics and P_T between the HL and the TL was identified. It was shown that, in 80% of the cases the received power for the link using the HL was at least 22 dB more than that of the TL-based Tx. To address the link asymmetry problem in V-VeLC systems, the paper proposed that a new system (or a protocol) design needs to be developed to improve the data throughput. In [11], the impact of vehicles' HL and TL illumination patterns on the communications performance between vehicles travelling on the same- and different- lanes was studied by developing a novel V-VeLC simulation model based on accurate empirical data measurements. Performance evaluation of V-VeLC was carried out based on the developed model, where the impact of the angle of incidence was analyzed based on the received signal strength, signal to noise ratio (SNR), and packet delivery ratio metrics. The authors reported that, using the TL, communications with vehicles on the adjacent lanes were possible only over a transmission range up to 10 m. From the foregoing, it is apparent that a robust Tx design is needed, which meets the requirements of the vehicular environment in terms of the communications range and the coverage area.

Some studies reported on infrared vehicular light communications (IR-VeLC) are also discussed as follows; In [12], a secure light communications protocol known as SecVLC, which is a cryptographic key generation/ management system, using the infrared (IR) and visible lights for link's security and data communications, respectively was proposed. In [13], a prototype vehicular light communications (VeLC) system with the IR-VeLC Tx mounted on the roof of a vehicle was reported with the focus being on the communications protocol for relaying transmitted data between vehicles. In [14], a RF and IR vehicle to vehicle communications system prototype for sending warning signals was demonstrated. However, none of the above works considered and analyzed the use of IR transmission for improving the link's robustness to the noise or increasing the communications transmission range considering realistic intervehicle distances.

Note that, in V-VeLC system the Sunlight induced noise is the major problem during the daytime, where the illumination level can be as much as 10 mW/cm^2 compared with uW/cm^2 for the intensity-modulated HL and TL [15]. This high-level of ambient light can lead to the saturated optical Rx. Note that, most works reported on V-VeLC have not considered the effect of Sunlight noise. Among the few reports that have considered the impact of Sunlight noise includes [16], where the impact of solar irradiance on VLC systems was investigated in terms of the BER, SNR degradation, and data rates. Results showed that, using an optical bandpass blue filter the link performance greatly improved over a short transmission span of up to 3 m. In [17] the effects of Sunlight irradiance and other external light sources on V-VeLC systems were investigated with regards to BER, data rates, and SNR over different months of the year, with and without an optical blue filter. Results obtained demonstrated a significant performance improvement in the achievable data rates and the average BER, e.g., in the month of January the average BER improved from 2×10^{-3} to $\sim 3 \times 10^{-5}$ using an optical blue filter. In addition, different noise cancellation methods such as wavelet-based signal processing and differential Rx-based hardware were proposed. However, due to the complexity of the processing, no real-time denoising has been demonstrated successful yet [9]. In [9], the effect of Sunlight noise on the performance of V-VeLC at a low speed of 30 km/h was considered. Note that, the effect of Sunlight noise becomes more significant as the link span increases, considering that the received power levels decrease with the increasing transmission distance. Moreover, to increase the transmission distance in V-VeLC, the use of converging lenses has been widely adopted. However, the higher the focal length *f* of the lenses used at the Rx the lower the angular field of view (AFOV) of the Rx, thereby reducing vehicle's maneuverability. Consequently, in this work we have considered practical VeLC channel, Tx, PD, lenses, and filter parameters. In addition, we have carried out BER performance analysis by considering a wide range of vehicle speeds and the Sunlight induced background noise (obtained

from solar irradiance measurements carried out in the city of Newcastle (N 54°59'44" W 1°39'52")).

It is noteworthy that, most works reported on V-VeLC are based on using a single light module, which may narrow down the conclusions drawn from the results. Therefore, in this work we characterize four TLs from different vehicles by measuring their radiation patterns and P_T. We also perform a link power budget analysis to determine the feasibility of V-VeLC using these TLs as the Txs for a range of TL irradiance angles with respect to the vehicle's speeds.

The main contributions of this work are:

- We present a channel model for VeLC where the Tx's specific radiant intensity model can be incorporated other than Lambertian radiant intensity model.
- We provide insights on the required horizontal and vertical AFOVs of the Rx for VeLC for the first time to the authors best knowledge.
- We show AFOV obtainable based on varying the PD sizes with varying *f* of lens and provide insights on the Tx's coverage diameter.
- We carry out optical characterization and performance evaluation of different vehicle TLs as Txs for VeLC systems.
- We propose a novel robust IR-VeLC system considering practical and realistic parameters.
- We carry out performance analysis of the proposed IR-VeLC with realistic Sunlight noise from empirical measurements.

The rest of the paper is organized as follows. In Section II the VeLC system is described while the configuration analysis is presented in Section III. Performance evaluation of V-VeLC system using TLs as Txs is given in Section IV. Section V describes the noise and BER analysis. The performance analysis of the proposed novel IR-VeLC is presented in Section VI. Finally, conclusions are given in Section VII.

II. The VELC System

Fig. 1(a)-(c) shows the composition of a typical VeLC system, which consists of the TL-based Tx (Vehicle 1) and the PD-based Rx (Vehicle 2). Note, for illustration purposes only a single TL is used. Including the second TL will have almost the same geometrical configuration, which results in the increased SNR at the Rx. Note, the Tx's positions with respect to the Rx and their beam profiles as well as the Rx's AFOV are very crucial in VeLC and will affect the link performance. For the line of sight (LOS) VeLC (Fig. 1(a)-(c)), the channel DC gain, which is the ratio of the received signal power at the Rx to the transmit power, can be expressed as:

$$H_{\mathrm{LOS}} = \begin{cases} \frac{A_{\mathrm{PD}} T_s(\varphi_{\mathrm{hor},\ \varphi_{\mathrm{ver}}}) g(\varphi_{\mathrm{hor},\ \varphi_{\mathrm{ver}}}) R_{\mathrm{Tx}}(\theta_{\mathrm{hor}}, \theta_{\mathrm{ver}})}{{L_S}^2}, \\ 0 \le \varphi_{\mathrm{hor}} \le \emptyset_{\mathrm{hor}} \text{ and } 0 \le \varphi_{\mathrm{ver}} \le \emptyset_{\mathrm{ver}} \\ 0, \ \varphi_{\mathrm{hor}} > \emptyset_{\mathrm{hor}} \ \text{ or } \varphi_{\mathrm{ver}} > \emptyset_{\mathrm{ver}} \end{cases} \tag{1}$$

where A_{PD} is the active area of the PD, φ_{hor} and φ_{ver} are the horizontal and vertical incidence angles, respectively, $R_{\mathrm{Tx}}(\theta_{\mathrm{hor}}, \theta_{\mathrm{ver}})$ is the radiation pattern (normalized beam profile) of the Tx at horizontal and vertical irradiance angles θ_{hor} and θ_{ver}, respectively, $\emptyset_{\mathrm{hor}}$ and $\emptyset_{\mathrm{ver}}$ denotes the horizontal and vertical AFOV semi angle of the Rx, L_S represents the link span, $T_s(\varphi_{\mathrm{hor},\ \varphi_{\mathrm{ver}}})$ and $g(\varphi_{\mathrm{hor},\ \varphi_{\mathrm{ver}}})$ are the gains of the optical filter (OF) and optical concentrator (OC), respectively. Note that, using (1) the Tx's specific radiation pattern can be incorporated, which may not be symmetrical as in Lambertian radiant intensity model. The gain of a non-imaging OC (NIOC) can be expressed as $A_{\mathrm{coll}}/A_{\mathrm{PD}}$ [18], where A_{coll} is the collection area of the NIOC.

Fig. 2 shows the system composition of an IR-VeLC system using an array of IR-LED as the light source at the Tx side. The OOK data stream is used for the intensity modulation of the Tx for transmission over the free space channel. At the Rx side, an OC, a narrow band optical band-pass filter (i.e., 810−890 nm) and an optical Rx are used to the regenerated electrical signal. For the LOS link, the received signal is given by [19]:

$$y\ (t) = \mathcal{R}x\,(t) \otimes\ h\,(t) + n\,(t), \tag{2}$$

where *R* is the responsivity of the PD, *x*(*t*) is the modulated light signal at the Tx, *h*(*t*) is the channel impulse response while *n*(*t*) denotes the additive white Gaussian noise including the Sunlight induced shot noise, which is the dominant noise source in VeLC during the daytime, the signal and dark current related shot noise sources and the thermal noise.

III. VeLC Configuration Analysis

A. Analysis of Horizontal/Vertical Semi-AFOV for VeLC With Imaging OC (IOC)

Using a convergent lens (i.e., IOC) at the Rx, as in a camera, an image of the Tx is captured on the PD-based sensor provided the Tx is within the Rx's AFOV. Note that, NIOCs do not produce an image of the Tx as do IOCs. First, we analyse the required horizontal semi-AFOVs (HS-AFOVs) for the Rxs 1 and 2 based on the worst-case scenario, where vehicles are located at the other sides of the lane, see Fig. 3. Note that, for the Rxs 1 and 2 to capture a single Tx and or two Txs the required HS-AFOV are φ_{12} , φ_{22}, φ_{11}, φ_{21}, respectively.

To obtain the required HS-AFOV between two vehicles travelling on the same lane, therefore we need to consider both the lane and vehicles' widths as well as the positions of the Rx and the Tx. Consequently, the required HS-AFOV for the Rx can be expressed as in (3)–(6) where w_{RL} is the width of the road lane, $L_{\mathrm{s-hor}}$ denotes the horizontal distance between the Tx and the Rx, w_{Tx}, and w_{Rx}, are the spacing between the Txs and the Rxs and, $w_{\mathrm{v-Tx}}$ and $w_{\mathrm{v-Rx}}$ are width of the vehicles, respectively and l_{Tx} denotes the length of the Txs (see Figs. 1 and 3). Note that, for the cases where one of the vehicles may move outside the lane, we replace w_{RL} by $w_{\mathrm{RL}} + x$ in (3)–(6), where x represents the deviation from the edge of the lane. Furthermore, (3)–(6) could be applied to vehicles on different lanes where w_{RL}becomes $2w_{\mathrm{RL}}$ or $3w_{\mathrm{RL}}$ for scenarios with one of the vehicles being on the next or the next two lanes, respectively.

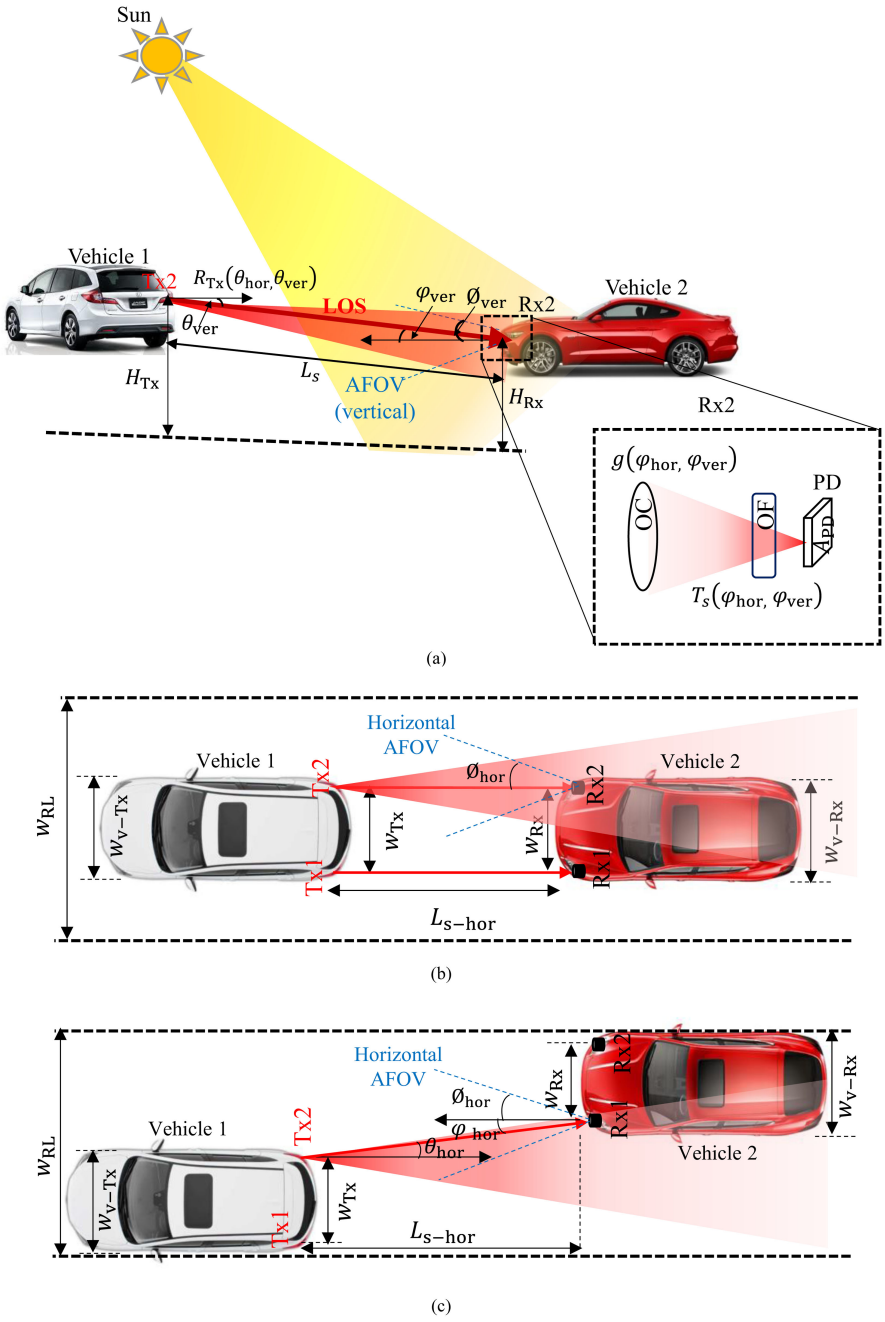

Fig. 1. VeLC configuration: (a) side view, (b) top view for perfect alignment scenario, and (c) top view with horizontal Tx and Rx misalignment (offset).

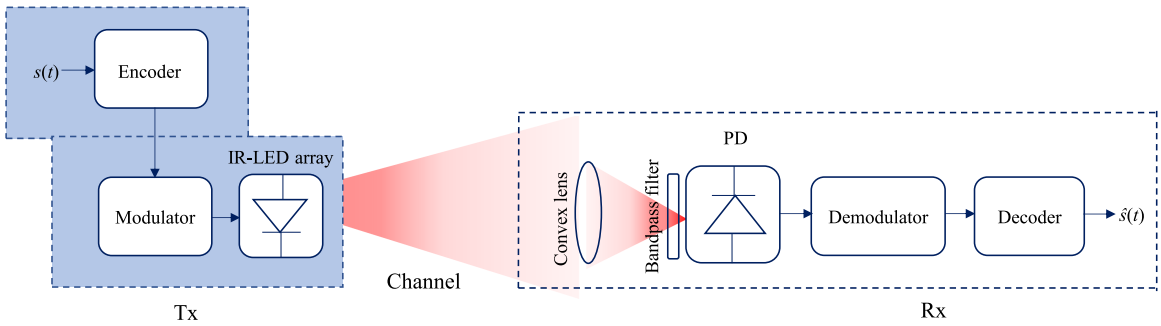

Fig. 2. The schematic system block diagram of an IR-VeLC system.

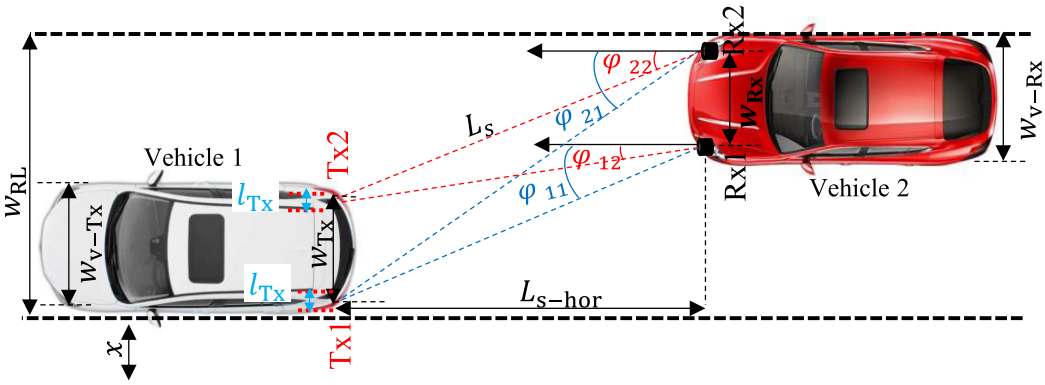

Fig. 3. VeLC configuration showing required horizontal AFOV.

$$\varphi_{12} = \arctan \left(\frac{w_{\mathrm{RL}} - \left(\frac{w_{\mathrm{v-Tx}} - w_{\mathrm{Tx}}}{2}\right) - \left(w_{\mathrm{Tx}} - \frac{l_{\mathrm{Tx}}}{2}\right) - \left(\frac{w_{\mathrm{v-Rx}} - w_{\mathrm{Rx}}}{2}\right) - w_{\mathrm{Rx}}}{L_{\mathrm{s-hor}}} \right), \tag{3}$$

$$\varphi_{22} = \arctan \left(\frac{w_{\mathrm{RL}} - \left(\frac{w_{\mathrm{v-Tx}} - w_{\mathrm{Tx}}}{2}\right) - \left(w_{\mathrm{Tx}} - \frac{l_{\mathrm{Tx}}}{2}\right) - \left(\frac{w_{\mathrm{v-Rx}} - w_{\mathrm{Rx}}}{2}\right)}{L_{\mathrm{s-hor}}} \right), \tag{4}$$

$$\varphi_{11} = \arctan \left(\frac{w_{\mathrm{RL}} - \left(\frac{w_{\mathrm{v-Tx}} - w_{\mathrm{Tx}}}{2}\right) + \frac{l_{\mathrm{Tx}}}{2} - \left(\frac{w_{\mathrm{v-Rx}} - w_{\mathrm{Rx}}}{2}\right) - w_{\mathrm{Rx}}}{L_{\mathrm{s-hor}}} \right), \tag{5}$$

$$\varphi_{21} = \arctan \left(\frac{w_{\mathrm{RL}} - \left(\frac{w_{\mathrm{v-Tx}} - w_{\mathrm{Tx}}}{2}\right) + \frac{l_{\mathrm{Tx}}}{2} - \left(\frac{w_{\mathrm{v-Rx}} - w_{\mathrm{Rx}}}{2}\right)}{L_{\mathrm{s-hor}}} \right). \tag{6}$$

The required vertical semi-AFOV (VS-AFOV) for the case shown in Fig. 1(a) is given as:

$$\varphi_{\mathrm{ver}} = \arctan \left(\frac{\Delta H}{L_{\mathrm{s-hor}}} \right), \tag{7}$$

where the offset between the Tx's and the Rx's vertical heights is $\Delta H = |H_{\mathrm{Tx}} - H_{\mathrm{Rx}}|$. The required HS- AFOV and VS-AFOV as a function of the link span for VeLC are depicted in Fig. 4, which is generated using (3)–(7) and the parameters given in Table I. From Fig. 4 it can be observed that, HS-AFOV exponentially drops with the link span. For example, for the Rx2 the required HS-AFOV increases by ~ 5 times as the link span decreased from 10 to 2 m. For the Rx1, the required HS-AFOV is lesser than the Rx2 due to it being closer to the Txs. Moreover, for VS-AFOV an exponential profile is also displayed with higher values for larger ΔH below the link span of 20 m.

Note that, increasing the vertical offset between the Tx and the Rx outside the vertical AFOV of the Rx will lead to increasing the vertical AFOV in order to capture the Tx while the horizontal AFOV requires no adjustment and vice versa.

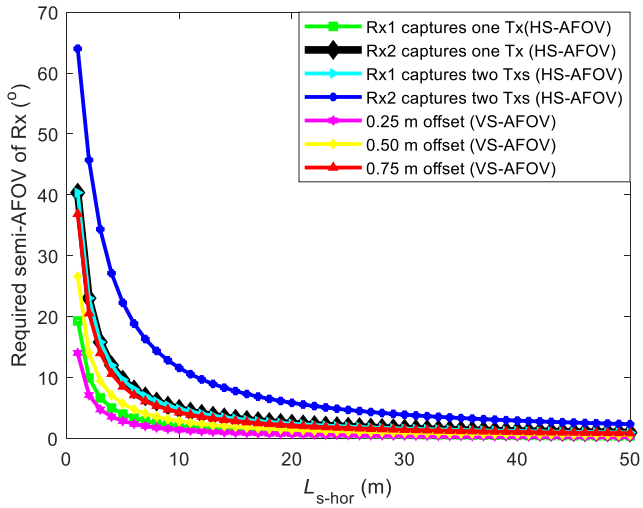

Fig. 4. The required HS-AFOV and VS-AFOV of Rx versus the $L_{\mathrm{s-hor}}$ for two vehicles on the same lane.

TABLE I
KEY GEOMETRY PARAMETERS AND SIMULATION VALUES

Parameter	Symbol	Value
Lane width	w_{RL}	2.5 m
Width of Tx vehicle	$w_{\mathrm{v-Tx}}$	1.7 m
Width of Rx vehicle	$w_{\mathrm{v-Rx}}$	1.7 m
Distance between Rx1 & Rx2	w_{Rx}	1.2 m
Distance between Tx1 & Tx2	w_{Tx}	1.2 m
Length of Txs	l_{Tx}	0.1 m
Horizontal link span	$L_{s-\mathrm{hor}}$	1-50 m
Vertical Tx and Rx offset	ΔH	0.25- 0.75 m
Lens focal lengths	f	25.4–50.0 mm
PD's surface area	A_{PD}	0.2 – ~2cm^2

B. Semi-AFOV Based on PD's Size and the Lens Focal Length

Using a convergent lens (i.e., IOC) to focus light onto the PD to increase the received optical power density results in reduced Rx's semi-AFOV, which needs investigating in terms of the PD's size and the f of lens, to meet the required semi-AFOV in vehicular communications, see Fig. 5. The semi-AFOV in

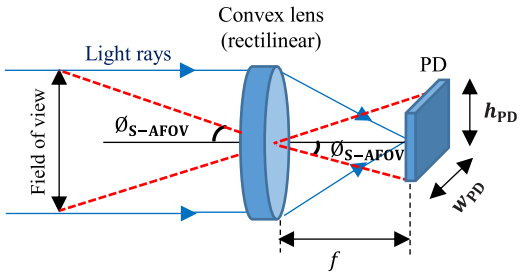

Fig. 5. Relationship between f, semi-AFOV and the PD size.

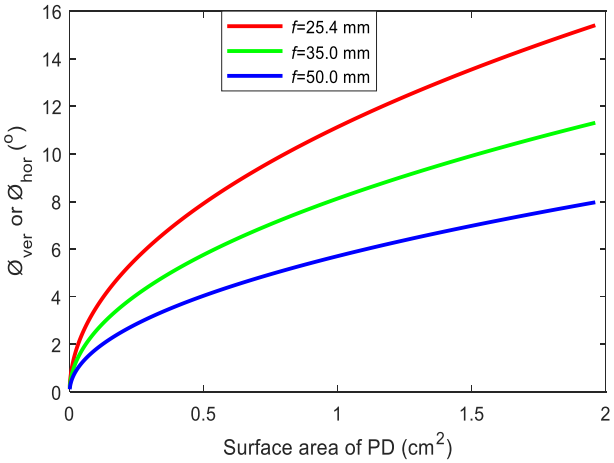

Fig. 6. $\emptyset_{\rm hor}$ or $\emptyset_{\rm ver}$ versus PD surface area for a range of f

terms of f and the PD's dimensions $D_{\rm PD}$ can be expressed as:

$$\emptyset_{\rm S-AFOV} = \arctan\left(\frac{D_{\rm PD}}{2f}\right), \tag{8}$$

$$\emptyset_{\rm S-AFOV} = \begin{cases} \emptyset_{\rm hor}, & D_{\rm PD} = w_{\rm PD}, \\ \emptyset_{\rm ver}, & D_{\rm PD} = h_{\rm PD}, \\ \emptyset_{\rm diag}, & D_{\rm PD} = \sqrt{{h_{\rm PD}}^2 + {w_{\rm PD}}^2}, \end{cases} \tag{9}$$

where $h_{\rm PD}$ and $w_{\rm PD}$ denotes the height and width of the PD and $\emptyset_{\rm hor}, \emptyset_{\rm ver}$ and $\emptyset_{\rm diag}$ is the horizontal, vertical and diagonal semi-AFOVs of the Rx, respectively.

Fig. 6 shows $\emptyset_{\rm hor}$ or $\emptyset_{\rm ver}$ as a function of the PD's surface area (where $w_{\rm PD} = h_{\rm PD}$) for a range of f. It can be seen that, using a convergent lens at the PD, $\emptyset_{\rm hor}$ or $\emptyset_{\rm ver}$ decreases with f and increases (logarithmic) with the PD's surface area.

C. Analysis of Tx's field of View (coverage profile)

Fig. 7 illustrates the Txs' beam coverage profile whereby L_1 depicts the horizontal distance from the Txs to the start of the overlapping light area between Txs 1 and 2, which can be expressed as:

$$L_1 = w_{\rm Tx}/(\tan\theta_{1/2-\rm in} + \tan\theta_{1/2-\rm out}), \tag{10}$$

where $\theta_{1/2-\rm in}$ and $\theta_{1/2-\rm out}$ are inner and outer half power angles of the Tx's beam, respectively, see Fig. 7. Note that, $\theta_{1/2-\rm in}$ and $\theta_{1/2-\rm out}$ of each Tx is the angle between the peak and the point on one side of the beam axis (left or right) where the received power is half the maximum. L_2 is the beam length of a single Tx

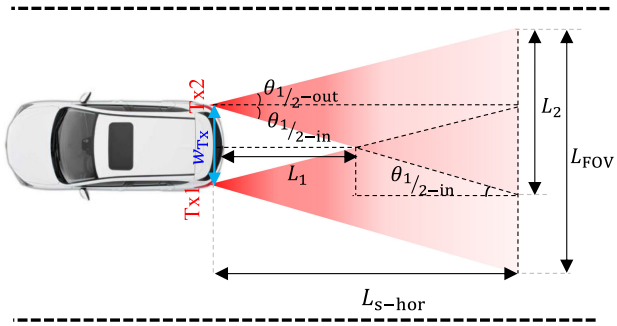

Fig. 7. Tx field of view (coverage diameter).

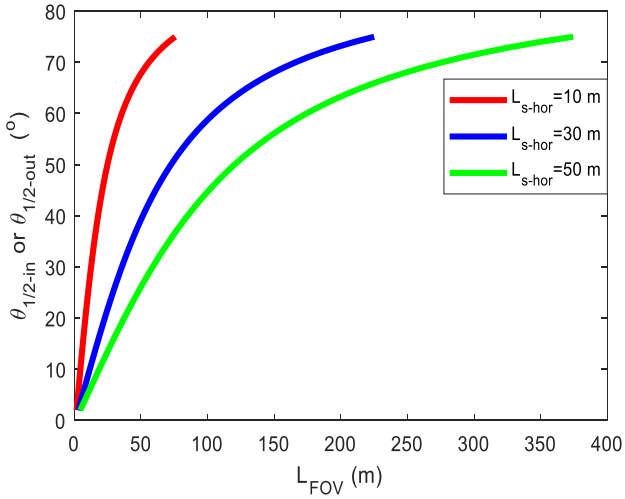

Fig. 8. Half power angle of Tx versus $L_{\rm FOV}$ for a range of $L_{\rm s\text{-}hor}$.

and $L_{\rm FOV}$ is the coverage length of both Txs beyond L_1, which can be expressed as:

$$L_2 = L_{s-\rm hor}\left(\tan\theta_{1/2-\rm in} + \tan\theta_{1/2-\rm out}\right), \tag{11}$$

$$L_{\rm FOV} = w_{\rm Tx} + L_{s-\rm hor}\left(\tan\theta_{1/2-\rm in} + \tan\theta_{1/2-\rm out}\right). \tag{12}$$

Note that, depending on $\theta_{1/2-\rm in}$ and $\theta_{1/2-\rm out}$ the light beams from Txs 1 and 2 may not overlap, therefore the coverage length is 2 $L_2 = 2L_{s-\rm hor}$ $(\tan\theta_{1/2-\rm in} + \tan\theta_{1/2-\rm out})$. Using (12), the half power angle (assuming $\theta_{1/2-\rm in} = \theta_{1/2-\rm out}$) versus the FOV for a range of link spans is depicted in Fig. 8, which shows a logarithmic increase of the Tx's half power angle with $L_{\rm FOV}$ reaching saturation points at ∼220 and ∼370 m for $L_{s-\rm hor}$ of 30 and 50 m, respectively. Note, the Tx's half angle decreases with the increasing link span.

IV. Performance Evaluation of V-VeLC With TLS-based Txs

Comprehensive performance analysis of the use of HLs with the given real beam patterns of different vehicle brands for data transmission was reported in [7]. The results showed that, the received power level increased with the decreasing Rx's heights from the ground due to the HLs being designed for road illumination points down-ward on the road surface as illustrated

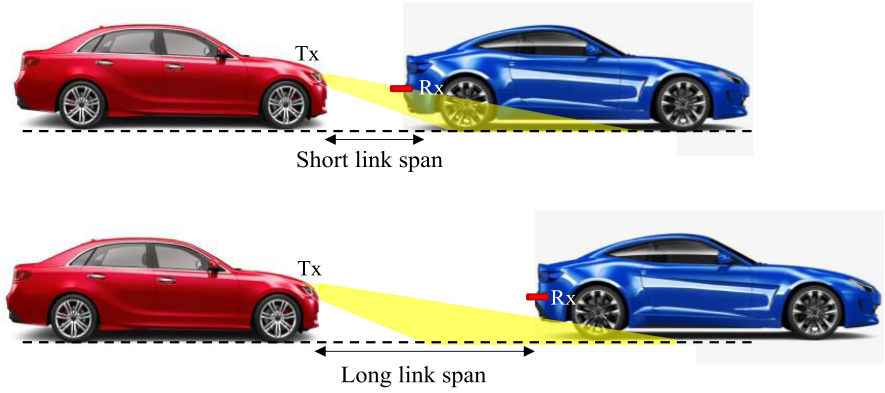

Fig. 9 V-VeLC links using HLs as the Txs.

TABLE II
TL PARAMETERS FROM EMPIRICAL MEASUREMENTS

TL	$\theta_{1/2-\text{in}}$ (°)	$\theta_{1/2-\text{out}}$ (°)	Illuminated area (cm^2)	P_T (mW)
BMW	75	65	124.7	110.5
Audi	55	47	46.2	39.7
Truck	10	10	80.0	32.4
Nissan	27	22	38.2	9.4

in Fig. 9. Consequently, this imposes the upper bound on the maximum transmission link span due to the angular inclination of the light rays on the road surface and its asymmetrical beam pattern. Most works reported on the use of TLs as Txs, are based on investigating the use of a single TL, which only outlines half the story, therefore, narrowing the conclusions drawn from the results obtained for the specific vehicle type/light model. No works have been reported on V-VeLC with different TL units. Therefore, to carry out performance evaluation of V-VeLC using TLs for data transmission we characterise four LED-based vehicle TLs for different vehicle modules.

A. Radiation Patterns of the TLs

First, we need to investigate the radiation patterns of the TLs, which defines the spatial intensity distribution of the emitted light from the TLs, which is important for the analysis of signal distribution and the coverage area. For this we have used a digital optical power meter (Thorlabs PM100D with a PD power sensor S120VC) to measure the received power levels over a fixed transmission distance of 1 m for a range of irradiance angle (i.e., -90^{o} (left) to $+90^{\text{o}}$ (right)) of the TLs. For comparison, we have used TLs from four popular vehicles namely: BMW F30 right side outer LED O/S TL (BMW TL), Audi A5 S5 N/S LED left outer TL facelift (Audi TL), Truck-DACA08712AM TL (Truck TL) and Nissan Qashqai right side tailgate boot lid TL 26550 4EA0A model (Nissan TL). We measured the radiation patterns for these TLs and the illuminated surface areas and estimated P_T, see Table II. As shown in Table II, the half power angle ($\theta_{1/2-\text{in}}$ and $\theta_{1/2-\text{out}}$) varies within the range of 10^{o} to 75^{o}, with the lowest and highest number for the Truck and BMW, respectively, which corresponds to the narrow and wide beam profiles as depicted in two-dimensional (2D) polar plots in Fig. 10.

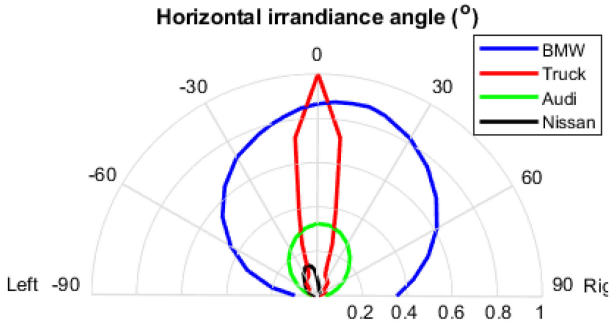

Fig. 10. 2D polar plots of the normalized beam profile of TLs from empirical measurements.

B. Link Power Budget Analysis

As part of the system design and implementation, we have carried out the link power budget analysis for V-VeLC using the four TLs units. For this, it is important to know the allowed inter-vehicle distances D_v for safe driving. Typically, a "two seconds" rule is recommended for D_v, whereby a driver maintains a minimum of two seconds behind the vehicle in front under the good weather condition, which is doubled to four seconds in bad weather conditions [20] as depicted in Fig. 11.

For a given P_T, the receiver power is given as:

$$P_r\ (\text{dBm}) = P_T\ (\text{dBm}) + H_{\text{LOS}}\,(\text{dB}) - L_{\text{sm}}\,(\text{dB}), \tag{13}$$

where L_{sm} is the link safety margin and H_{LOS} is the channel DC gain for the LOS, which is given by:

$$H_{\text{LOS}}\,(\text{dB}) = 10\log_{10}(A_{\text{PD}}\,T_s\,(\varphi_{\text{hor}},\,\varphi_{\text{ver}})\,g\,(\varphi_{\text{hor}},\,\varphi_{\text{ver}})\,R_{\text{Tx}}\,(\theta_{\text{hor}},\theta_{\text{ver}})\,/{D_v}^2), \tag{14}$$

Table III shows the key parameters used for the link power budget analysis. Figure 12 shows the received power (in dBm) per Tx against the vehicles' speed for a range of irradiance angle

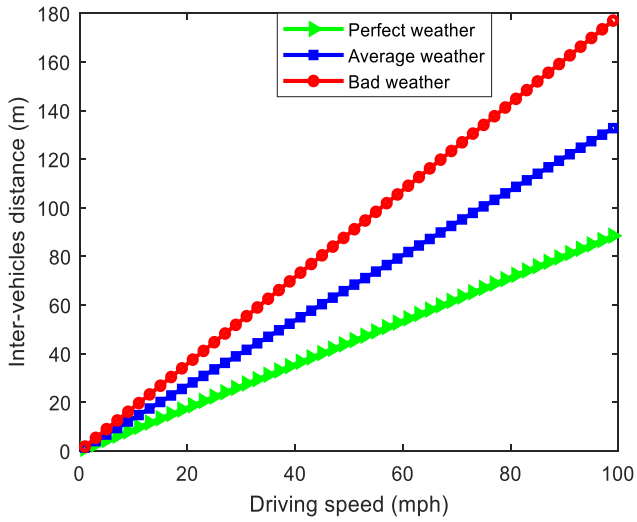

Fig. 11. The inter-vehicle distance as a function of driving speeds using the 2 seconds driving rule.

TABLE III
KEY PARAMETERS OF THE LINK POWER BUDGET ANALYSIS

Parameter	Symbol	Value
Link safety margin	L_{sm}	3 dB
Surface area of PD	A_{PD}	1.5 cm^2
TL transmit power	P_T	9.4-110.5 mW
Irradiance angle	$[\theta_{\text{hor}}, \theta_{\text{ver}}]$	[0°, 0°]- [20°, 0°]
Inter-vehicle distance	D_v	1- ~90 m
Diameter of NIOC	d	25.4 mm-50.0 mm
Vehicle speed	S	~1-100 mph
Gain of optical filter	$T_s(\varphi_{\text{hor}}, \varphi_{\text{ver}})$	1

TABLE IV
SUMMARY OF ACHIEVABLE DRIVING SPEEDS AND INTER-VEHICLE DISTANCES AS $[\theta_{hor}, \theta_{ver}]$ INCREASES FROM [0°, 0°] TO [20°, 0°]

TL type	$[\theta_{\text{hor}}, \theta_{\text{ver}}]$ =[0°, 0°]		$[\theta_{\text{hor}}, \theta_{\text{ver}}]$= [20°, 0°]	
	Speed (mph)	D_v (m)	Speed (mph)	D_v (m)
BMW	6.4	5.7	6.2	5.5
Audi	4.0	3.6	3.7	3.3
Truck	3.6	3.2	1.2	1.1
Nissan	1.7	1.5	2.2	2.0

$[\theta_{\text{hor}}, \theta_{\text{ver}}]$ of [0°, 0°] to [20°, 0°] (left of the TL's beam axis), for the case with no OC at the Rx. The figure reveals that, for the BMW TL the maximum driving speed is 6.4 mph (i.e., D_v = 5.7 m) for $[\theta_{\text{hor}}, \theta_{\text{ver}}]$ = [0°, 0°] and P_r of −36 dBm (i.e., for a receiver sensitivity of -36 dBm), while for Truck TL there is a sharp decrease in the achievable driving speeds from 3.6 to 1.2 mph as $[\theta_{\text{hor}}, \theta_{\text{ver}}]$ increases from [0°, 0°] to [20°, 0°] due to its narrower radiation pattern. A summary of the attainable driving speeds and D_v for TLs under study are given in Table IV. Note, these achievable speeds are far lower than the typical recommended vehicle's speed limits, e.g., for cars, motorcycle, vans and buses a driving speed of 30, 60, 70 and 70 mph is approved in built-up areas, single carriage ways, dual carriage ways and motorways (mph), respectively [21]. Fig. 13 illustrate the predicted required P_T against the driving speed for cases with and without the OC at the Rx. Note, the required P_T drops by 5.3, 8.1 and 11.2 dB when a NIOC with the diameter d of 25.4, 35.0 and 50.0 mm are used at the PD, respectively.

V. NOISE AND BER ANALYSIS

A. Ambient Noise

In VeLC, there are two main ambient light induced noise sources of (*i*) the streetlights (at night), advertising boards and other vehicle lights; and (*ii*) the background solar radiation (Sunlight), which is the dominant noise source. Note that, the solar irradiance $P_{\text{solar}}(\lambda)$ varies by the time of the day and latitude, i.e., the position of the sun. In addition, its effect on the performance of VeLC system will depend on the direction and orientation of the Rx. The photocurrent generated at the PD due to $P_{\text{solar}}(\lambda)$ is given as:

$$I_{\text{solar}} = A_{\text{PD}}\, g\left(\varphi_{\text{sun}}\right) \cos\left(\varphi_{\text{sun}}\right) G_{\text{PD}} \int_{\lambda_1}^{\lambda_n} P_{\text{solar}}\left(\lambda\right) T_f\left(\lambda\right) \mathcal{R}\left(\lambda\right) d\lambda, \tag{15}$$

where A_{PD} and G_{PD} are the active area and gain of the PD, respectively, φ_{sun} is the difference in the orientation angle between that of the measured $P_{\text{solar}}(\lambda)$ and the PD, λ_1 and λ_n are the integration limits, i.e., the wavelength band, which are 405–690 nm and 810–890 nm for visible and IR-based systems, respectively. The gain of the OC is denoted as $g(\varphi_{\text{sun}})$, $\mathcal{R}(\lambda)$ is the responsivity of the PD and $T_f(\lambda)$ is the optical band pass filter's transmittance. Note that, the daytime background radiation-induced shot noise is the dominant noise source in VeLC, which can be expressed as [22], [23]:

$$\sigma^2_{\text{bgr}} = 2q_e I_{\text{solar}} B, \tag{16}$$

where q_e is the electron charge and B is the system bandwidth.

B. Thermal and Shot Noise Sources

Thermal noise is generated due to the random motion of charge carriers [9] and its variance is given as [23], [24]:

$$\sigma^2_{\text{thermal}} = \frac{4kT_K B}{R_L}, \tag{17}$$

where k is the Boltzmann's constant, T_K is the absolute temperature in Kelvin and R_L is the load resistance.

Note that, the photodetection process, which is discrete in nature, results in the signal-dependent shot noise at the PD [25], [26], with the variance given as [26]:

$$\sigma^2_{\text{shot-rs}} = 2q_e \mathcal{R}\left(\lambda\right) P_r B, \tag{18}$$

where P_r is the average received signal power (i.e., desired signal). In addition, the PD's dark current noise variance is given as [23]:

$$\sigma^2_{\text{dk}} = 2q_e I_{\text{dk}} B, \tag{19}$$

where I_{dk} is the dark current.

The total noise variance is then given as:

$$\sigma^2_T = \sigma^2_{\text{bgr}} + \sigma^2_{\text{thermal}} + \sigma^2_{\text{shot-rs}} + \sigma^2_{\text{dk}}. \tag{20}$$

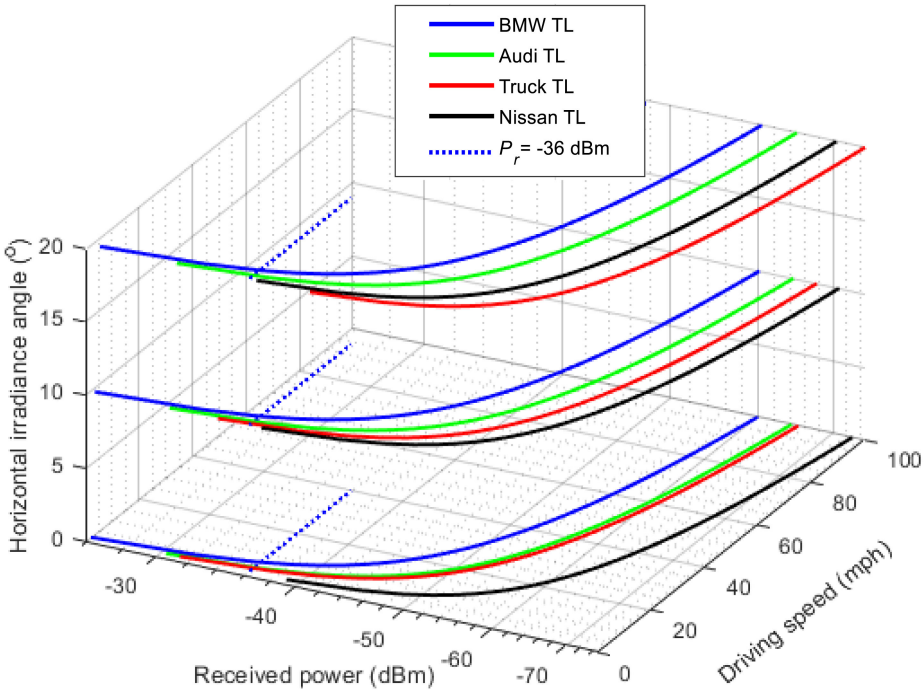

Fig. 12. The horizontal irradiance angle as a function of the received power and driving speed for different TLs.

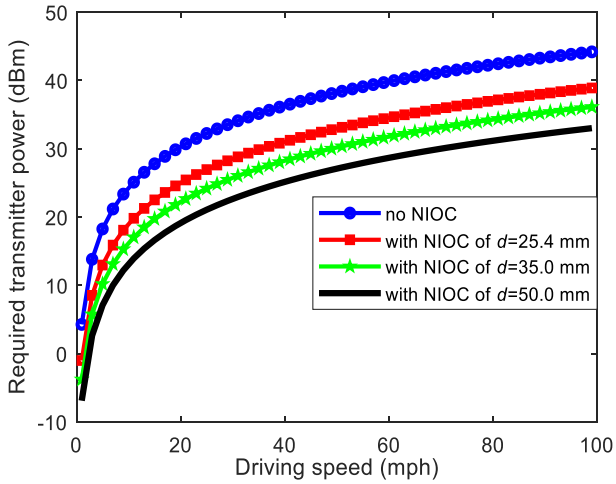

Fig. 13. The required transmit power versus the driving speed for the system with and without a NIOC.

C. BER

In this work, we have adopted the intensity modulation direct detection scheme with OOK and a PD (Hamamatsu S6968) as the Rx. Once the relative positions of the Tx and the Rx are ascertained, the minimum received optical power (i.e., considering a single Tx) and the noise variances of thermal noise, ambient, signal and dark current shot noises are obtained using (13), (15)–(19). Note that, the systems bandwidth is primarily determined by the low pass filter characteristics of the Rx, which is $B = R_b/2$, where R_b is the data rate [24]. Consequently, for the additive white Gaussian noise channel, the SNR at the Rx is given by [19]:

$$\mathrm{SNR} = \frac{(\mathcal{R}(\lambda) P_r)^2}{\sigma_T^2}. \tag{21}$$

Thus, the BER is then given as [19]:

$$\mathrm{BER} = Q\left(\sqrt{\mathrm{SNR}}\right), \tag{22}$$

where $Q(x)$ is the Q-function used for the calculation of the tail probability of the standard Gaussian distribution given by [19]:

$$Q(x) = \frac{1}{\sqrt{2\pi}} \int_x^\infty e^{\frac{-y^2}{2}} dy. \tag{23}$$

VI. Performance Analysis of IR-VeLC

Here, we have used an array of IR-LED (Osram SFH 4715AS) with a symmetrical light pattern and no angular inclination towards the road surface for the vehicle IR-light Txs in order to meet the driving speed (i.e., typical inter-vehicle distances) requirements. First, we show the received power per Tx over driving speeds for a range of d by numerical simulations using (13) and (14). Note, (*i*) only LOS is considered since the Tx is a symmetrical light source with no angular inclination towards the road, thus with no significant reflections from the road surface; and (*ii*) the transmit optical power level must meet the IEC 62471/2006 emission limits for eye safety, which specifies emission limit of 100 W/m^2 [27], whereas the proposed system in this work has a maximum of 5.92 W/m^2 (for the two front/rear Txs) at 1 m distance from the Txs. The key system parameters adopted in this work are provided in Table V.

It is important to note that, the greatest challenge in VeLC systems is to ensure link robustness under strong ambient light.

TABLE V
KEY SYSTEM PARAMETERS

Parameter	Symbol	Value
Active area of PD (Rx)	A_{PD}	1.5 cm^2
Peak wavelength of LED	λ	860 nm
Inter-vehicle distance	D_v	1- ~90 m
Absolute temperature	T_K	298 K
System bandwidth	B	1-5 MHz
Responsivity of PD at 850nm & 640nm (i.e. for IR-LED & BMW TL, respectively)	$\mathcal{R}(\lambda)$	0.63 & 0.44 A/W
Solar irradiance	P_{solar}	413.77 W/m^2
Load resistance	R_L	50 ohms
Maximum PD dark current	I_{dc}	5 nA
Transmission coefficient of filter	$T_f(\lambda)$	1
Vehicle speed		2- 100 mph
Half power angle of IR-LED		$\pm 45^{\circ}$
Transmit power per IR-LED		1.34 W
Number of LEDs per Tx		7
PD model (Hamamatsu (Si PIN))		S6968
LED model (Osram)		SFH 4715AS
IR bandpass filter model (Thorlabs)		FB850-40
Visible bandpass filter (MidOpt)		BP550

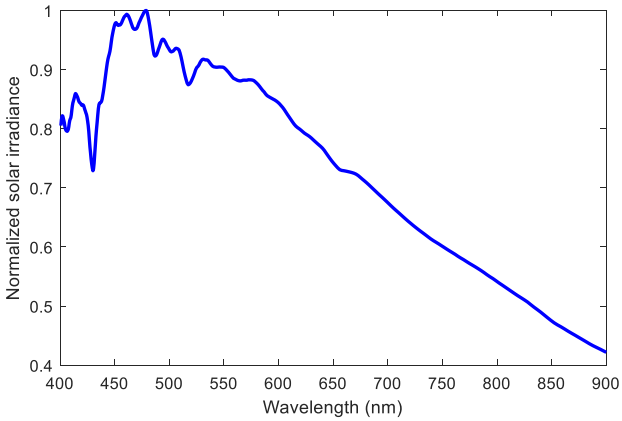

Fig. 14. Normalized solar irradiance as a function of wavelength.

Consequently, we propose an IR-VeLC system to mitigate this challenge for the following reasons: (*i*) Sunlight irradiance in the IR band is much lower than the visible band, which leads to improved signal to noise ratio performance. For example, from Fig. 14 (data source from [28]), in the IR region at the wavelength of 850 nm, the solar irradiance is less than 50% compare to the wavelength of 480 nm in the visible light region; and (*ii*) the incorporation of IR-LEDs will help to meet the required transmit power level (within safety limits) needed for longer distance transmissions, where the TLs would not be able to offer, see Section IV. Note, the high or low beam HLs, which have higher transmit powers than TLs are only used at night or when the visibility is low due to fog, heavy rain, snow, etc., thus imposing limitation in V-VeLC systems. The proposed work overcomes these issues and limitations by introducing the use of IR-LEDs in addition to HLs and TLs, to ensure link availability at all times and can come on when data is being transmitted unnoticeable to the human eyes. In addition, there are other merits of IR-LEDs such as (*i*) the electrical-to-optical conversion efficiency of IR-LEDs are higher than the visible blue LED-based white light

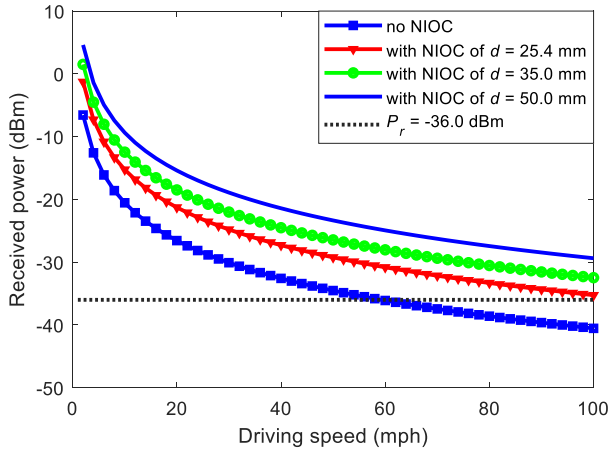

Fig. 15. Received power against the driving speeds for the Rx with and without a NIOC.

sources [29]; and (*ii*) the 3 dB bandwidth of IR-LEDs are higher than the white LEDs, which is well known [29].

The plots of the received power against the driving speed for the case with and without an OC at the Rx is depicted in Fig. 15. It can be seen that, the received power increases and decreases with d and the driving speed, respectively. For example, at P_r of -36 dBm without an OC and with a NIOC of d = 25.4 mm, the driving speeds are 60 and ~100 mph, respectively. Note that, the received power increases by 5.3, 8.1 and 11.2 dB using a NIOC with d of 25.4, 35.0 and 50.0 mm, respectively.

The predicted BER performance as a function of the driving speed for the proposed IR-VeLC system using IR-LEDs and BMW TL (chosen because it has the highest P_T among the four TLs characterized) for a range of data rates is shown in Fig. 16 via numerical simulations using (15)–(23). Here we have considered P_{solar} of 413.77 W/m^2, NIOC with d of 25.4 mm and a narrow bandpass filter (Thorlabs FB850-40) at the Rx. Note, a solar power meter (ISO-TECH ISM410) was used to measure the solar irradiances (wavelength range of 400-1100 nm) at the various positions with respect to the Sun. $P_{\text{solar}}(\lambda)$ for the direction with the highest average value (measured at the city of Newcastle, U.K., N 54°59'44" W 1°39'52") is used in our simulations. Note, the Rx is located on the vehicle pointing towards the vehicles on the road with no horizontal tilting angle.

As can be observed from Fig. 16, BMW TL does not meet typical driving speeds limits (i.e., inter-vehicle link spans) due to low P_T. Note, only driving speeds of 7, ~6 and 5 mph (translating to a L_S of 6.3, 5.4 and 4.5 m, respectively) are achievable at R_b of 2, 6 and 10 Mbps, respectively, at the FEC BER limit of 3.8 $\times 10^{-3}$. However, the proposed system with the IR-LEDs offers driving speeds of >100, 80 and 70 mph (translating to a L_S >89, 72 and 63 m) at R_b of 2, 6 and 10 Mbps, respectively under the same conditions and a high ambient light level. Note, a sharp increase in the BER with respect to the driving speed up to ~ 60, ~70 and ~90 mph for the links with R_b of 10, 6 and 2 Mbps, respectively. For example, at R_b of 10 Mbps the BER values are 8.0 $\times$ 10^{-8} and 3.8 $\times$ 10^{-3} for the driving speed of 50 and ~70 mph, respectively. This is because,

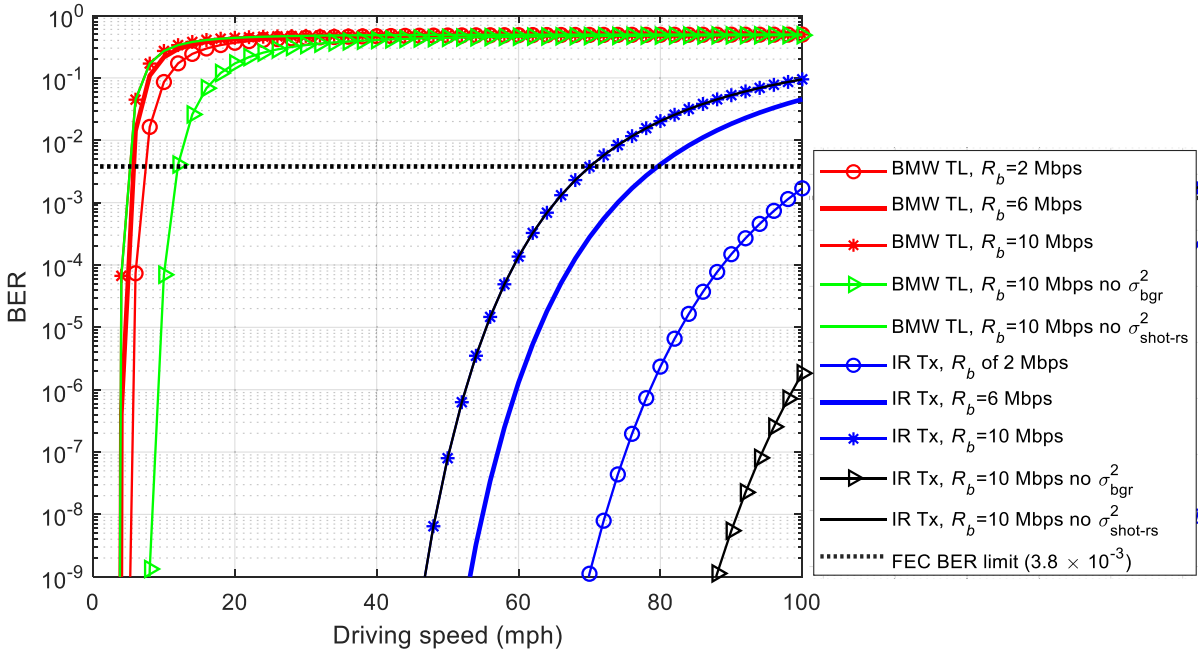

Fig. 16. The BER performance against the driving speed for a range of *Rb* for the proposed vehicular IR-VeLC system.

the received power level reduced by ∼50% (i.e., from 1.2 μW (−29.2 dBm) to 0.6 μW (−32.2 dBm)).

Moreover, to demonstrate the impact of the noise on the link performance we investigate the BER for BMW TL and the proposed IR-VeLC system by considering all noise sources as in (20) without the (*i*) Sunlight noise $\sigma^2_{\rm bgr}$; and (*ii*) signal dependent shot noise $\sigma^2_{\rm shot-rs}$, see Fig. 16. For example, for the proposed IR-VeLC system, the BER at a driving speed of 90 mph without and with $\sigma^2_{\rm bgr}$ are 5.5 $\times 10^{-9}$ and 5.3 $\times 10^{-2}$, respectively. For the link using BMW TL, the BER at the speed of 8 mph without and with $\sigma^2_{\rm bgr}$ are 1.3 $\times 10^{-9}$ and 1.7 $\times 10^{-1}$, respectively. As shown in Fig. 16, $\sigma^2_{\rm shot-rs}$ has negligible impact on the BER performance compared with $\sigma^2_{\rm bgr}$.

VII. Conclusion

We carried out a performance evaluation study on the use of different vehicle TLs as Txs for V-VeLC systems. The results obtained showed that, the radiation characteristics and P_T are not the same for different vehicle TLs, thus impacting the coverage area, signal distribution and the communication distance, which are key factors in the practical deployment of VeLC as part of ITS. Consequently, based on the obtained results we proposed the incorporation of IR-LEDs in vehicle HLs and TLs to meet the typical communication link spans in vehicular environments. We showed that, the proposed IR-VeLC system offers improved performance particularly under Sunlight compared with the visible lights-based TLs. We showed that, at the target FEC BER limit of 3.8 $\times 10^{-3}$, transmission distances up to 63, 72 and >89 m were achieved by the proposed IR-VeLC compared with 4.5, 5.4 and 6.3 m for BMW vehicle-based TL at data rates of 10, 6 and 2 Mbps, respectively. Furthermore, the proposed scheme deals with the link asymmetry highlighted in [10] in section I, since both the front and rear vehicle's Txs will have the same P_T and radiation characteristics. Moreover, we analyzed the maximum HS-AFOV and VS-AFOV required for vehicles traveling on the same lanes to establish data communication, based on the road lane width and the positions of the Txs and Rxs on the vehicles (with an imaging-based OC at the Rx).

References

[1] E. Eso *et al.*, "Experimental demonstration of vehicle to roadside infrastructure visible light communications," in *Proc. 2nd West Asian Colloquium On Optical Wireless Communications (WACOWC)*, Tehran, Iran, 2019, pp. 85–89.

[2] A. Memedi, C. Tebruegge, J. Jahneke, and F. Dressler, "Impact of vehicle type and headlight characteristics on vehicular VLC performance," in *Proc. IEEE Veh. Netw. Conf. (VNC)*, Taipei, Taiwan, 2018, pp. 1–8.

[3] Y. Zhou *et al.*, "Service-aware 6G: An intelligent and open network based on the convergence of communication, computing and caching," *Digit. Commun. Networks*, vol. 6, no. 3, 2020, pp. 253–260.

[4] Y. Zhou, L. Tian, L. Liu, and Y. Qi, "Fog computing enabled future mobile communication networks: A convergence of communication and computing," *IEEE Commun. Mag.*, vol. 57, no. 5, pp. 20–27, May 2019.

[5] M. Katz and I. Ahmed, "Opportunities and challenges for visible light communications in 6G," in *Proc. 2nd 6G Wireless Summit (6G SUMMIT)*, Levi, Finland, 2020, pp. 1–5.

[6] M. Z. Chowdhury, M. Shahjalal, M. K. Hasan, and Y. M. Jang, "The role of optical wireless communication technologies in 5G/6G and IoT solutions: Prospects, directions, and challenges," *Appl. Sci.*, vol. 9, no. 20, pp. 4367, Oct. 2019.

[7] P. Luo, Z. Ghassemlooy, H. L. Minh, E. Bentley, A. Burton, and X. Tang, "Performance analysis of a car-to-car visible light communication system," *Appl. Opt.*, vol. 54, no. 7, pp. 1696–1706, 2015.

[8] M. Elamassie, M. Karbalayghareh, F. Miramirkhani, R. C. Kizilirmak, and M. Uysal, "Effect of fog and rain on the performance of vehicular visible light communications," in *Proc. IEEE 87th Veh. Technol. Conf. (VTC Spring)*, Porto, 2018, pp. 1–6.

[9] H. Farahneh, F. Hussain, and X. Fernando, "Performance analysis of adaptive OFDM modulation scheme in VLC vehicular communication network in realistic noise environment," *J. Wireless Commun. Netw.*, vol. 2018, pp. 243, 2018.

[10] H. Y. Tseng, Y. L. Wei, A. L. Chen, H. P. Wu, H. Hsu, and H. M. Tsai, "Characterizing link asymmetry in vehicle-to-vehicle Visible Light Communications," in *Proc. IEEE VNC*, Kyoto, Japan, 2015, pp. 88–95, doi: 10.1109/VNC.2015.7385552.
[11] A. Memedi, H.-M. Tsai, and F. Dressler, "Impact of realistic light radiation pattern on vehicular visible light communication," in *Proc. IEEE GLOBECOM*, Singapore, 2017.
[12] B. Turan and S. Ucar, "Vehicular visible light communications," *Intechopen.*, 2017, doi: 10.5772/intechopen.69536. [Online]. Available: https://www.intechopen.com/books/visible-light-communications/vehicular-visible-light-communications.
[13] H. Fujii, O. Hayashi, and N. Nakagata, "Experimental research on inter-vehicle communication using infrared rays," *Proc. Conf. Intell. Veh.*, Tokyo, Japan, 1996, pp. 266–271.
[14] E. Hossain, N. Mamun, and M. F. Faisal, "Vehicle to vehicle communication using RF and IR technology," in *Proc. 2nd Int. Conf. Elect. Electronic Eng. (ICEEE)*, RUET, Rajshahi, Bangladesh, 2017, pp. 27–29.
[15] A. Căilean and M. Dimian, "Current challenges for visible light communications usage in vehicle applications: A survey," *IEEE Commun. Surv. Tut.*, vol. 19, no. 4, pp. 2681–2703, Fourthquarter 2017.
[16] M. S. Islim *et al.*, "The impact of solar irradiance on visible light communications," *J. Lightw. Technol.*, vol. 36, no. 12, pp. 2376–2386, 2018.
[17] H. Farahneh, S. M. Kamruzzaman, and X. Fernando, "Differential receiver as a denoising scheme to improve the performance of V2V-VLC systems," in *Proc. IEEE Int. Conf. Commun. Workshops (ICC Workshops)*, KS City, MO, 2018, pp. 1–6.
[18] Z. Ghassemlooy, L. N. Alves, S. Zvanovec, and M. A. Khalighi, "Visible light communications: Theory and applications," CRC, 2017.
[19] J. M. Kahn and J. R. Barry, "Wireless infrared communications," *Proc. IEEE*, vol. 85, no. 2, pp. 265–298, Feb. 1997.
[20] "The two-second rule". Road safety authority (Government of Ireland). Available at: //web.archive.org/web/20120309213451/http://www.rotr.ie/rules-for-driving/speed-limits/speed-limits_2-second-rule.html
[21] 'Speed limits'. United Kingdom government. [Online]. Available: https://www.gov.uk/speed-limits
[22] T. Komine and M. Nakagawa, "Fundamental analysis for visible-light communication system using LED lights," *IEEE Trans. Consum. Electron.*, vol. 50, no. 1, pp. 100–107, Feb. 2004.
[23] R. Hui, *Introduction to Fiber-Optic Communication*, New York, Orlando, FL: Academic, San Diego, CA, 2020, pp. 125–154.
[24] O. Haddad, M. A. Khalighi, and S. Zvanovec, "Channel characterization for optical extra-WBAN links considering local and global user mobility," *SPIE OPTO*, San Francisco, USA: Academic, Feb. 2020.
[25] R. Paudel, "Modelling and analysis of free space optical link for Ground-to-Train communications," *Department of Mathematics, Physics and Electrical Engineering PhD dissertation*, Northumbria Univ. 2014.
[26] R. Hui and M. O'Sullivan, *Fiber Optic Measurement Techniques*, New York, Orlando, FL, San Diego, CA: Academic, 2009, pp. 1–128.
[27] I. E. Commission, "IEC-62471: Photobiological safety of lamps and lamp systems," s.l.: IEC, 2006. Table 6.1. CIE/IEC-62471:2006.
[28] CSIM Solar Spectral Irradiance, Time series, "Lasp interactive solar irradiance datacentre." [Online]. Available: https://lasp.colorado.edu/lisird/data/csim_ssi_l3/
[29] S. M. Mana, P. Hellwig, J. Hilt, P. W. Berenguer, and V. Jungnickel, "Experiments in Non-Line-of-Sight li-fi channels," in *Proc. Global LIFI Congr. (GLC)*, Paris, France, 2019, pp. 1–6.

Elizabeth Eso (Member, IEEE) received the B.Eng. degree in electrical and electronics engineering from Abubakar Tafawa Balewa University, Bauchi, Nigeria, in 2011 and the M.Sc. degree in microelectronics and communications engineering from Northumbria University, Newcastle upon Tyne, U.K., in 2014 with Distinction. In 2016, she joined the Federal University of Technology, Akure, Nigeria, as an Academic Staff. She is currently a Ph.D. Researcher with the Optical Communications Research Group, Northumbria University with a Marie Curie Fellowship. Her research interest includes visible light communications, optical camera communications, and free space optics. She was the Second Prize Winner in the IEEE Students Project Presentation Competition in the North East Region Network, U.K. in 2014.

Zabih Ghassemlooy (Senior Member, IEEE) received the B.Sc. (Hons.) degree in EE engineering from Manchester Metropolitan University, Manchester, U.K., in 1981, and the M.Sc. and Ph.D. degrees from The University of Manchester, Manchester, U.K., in 1984 and 1987, respectively. During 1987–1988, he was a Postdoctoral Research Fellow with City University, U.K. During 2004–2014, he joined the Faculty of Engineering and Environment, Northumbria University, Newcastle upon Tyne, U.K., as an Associate Dean Research. He is currently the Head of Optical Communications Research Group. In 2016, he was a Research Fellow and in 2015, a Distinguished Professor with the Chinese Academy of Science, Beijing, China. He has authored or coauthored more than 900 papers, including more than 350 journals and eight books, 100 keynote or invited talks and supervised ten Research Fellows and 65 PhDs. His research interests include optical wireless communications, free space optics, visible light communications, hybrid RF, and optical wireless communications. He is the Chief Editor of the *British Journal of Applied Science and Technology* and the *International Journal of Optics and Applications*. Since 2018, he has been the Vice-Chair of the OSA Technical Group of Optics in Digital Systems.

Stanislav Zvanovec (Senior Member, IEEE) received the M.Sc. and Ph.D. degrees from Czech Technical University (CTU) in Prague, Prague, Czechia, in 2002 and 2006, respectively. He is currently a Full Professor and the Deputy Head of the Department of Electromagnetic Field and leader of Wireless and Fiber Optics team, CTU. He is the author of two books and more than 250 journal articles and conference papers. His current research interests include free space optics (FSO) and fiber optical systems, visible light communications (VLC), and RF over optics.

Juna Sathian received the Ph.D. degree from the Queensland University of Technology (QUT), Brisbane, QLD, Australia, in 2013. In 2014, she was a Postdoctoral Research Associate with the Department of Materials, Imperial College London, London, U.K., where she was a Key Researcher and Co-Developer of the world's first room-temperature continuous wave maser (in diamond). During this time, she worked on high brightness solid-state light sources (LED-pumped luminescent concentrator) and novel precision wavelength-tunable diode-pumped Alexandrite laser technology. In 2019, she was a Senior Lecturer with the Department of Mathematics, Physics, and Electrical Engineering, University of Northumbria, Newcastle, U.K. Her current research interests include laser technology, room-temperature maser technology, luminescent concentrator light technology for high brightness applications, and visible light communication with focus on healthcare applications. She is a Member of the Institute of Physics (IOP).

Asghar Gholami received the B.Sc. and M.Sc. degrees in electronics engineering from the Isfahan University of Technology (IUT), Isfahan, Iran, in 1993 and 1996, respectively, and the Ph.D. degree in electrical engineering from Ecole Supérieure d'Electricité (Supélec), France, in 2003. In 2008, he joined Draka Communications in the Fiber Product Technology, Marcoussis, France. Since 2009, he has been with the Department of Electrical and Computer Engineering, IUT, Isfahan, Iran. He has authored and coauthored more than 40 papers and holds more than five US patents. His research interests include optoelectronics and optical wireless communications. He was the recipient of the Postdoctoral Fellowship by Supélec University in 2007.